Dual-Band Circular-Polarized Microstrip Antenna for Ultrawideband Positioning in Smartphones With Flexible Liquid Crystal Polymer Process

Yongjian Zhang, Yue Li, *Senior Member, IEEE*, Mingzhe Hu, Pengfei Wu, and Hanyang Wang, *Fellow, IEEE*

***Abstract*— This article proposes a dual-band circular-polarized (DBCP) microstrip antenna using flexible liquid crystal polymer (LCP) manufacturing process for ON-smartphone ultrawideband (UWB) positioning application. To achieve dual-band circular polarization in a low profile, the proposed antenna is designed with a cross-slot-loaded patch with four L-shaped feeding probes and a sequential phase feeding network. A circle of capacitive via fence is loaded surrounding the patch for area miniaturization, which is adaptive for the limited space of flexible printed circuit (FPC) in smartphones. Based on the UWB positioning protocol, a three-element antenna array is constructed in a low profile of $0.015\lambda_0$ with required isolation of 17 dB. Experimental results show the overlapped bandwidth of the efficiency and the axial ratio (AR) covering the demand bands of 6.30–6.80 and 7.75–8.10 GHz. With the properties of dual wideband operation, circular polarization, and ultralow profile, the proposed antenna exhibits feasible solutions for the UWB positioning application in space-limited smartphones.**

***Index Terms*— Antenna array, antenna feeding, circular polarization, microstrip antennas, multiple-band antennas.**

I. Introduction

With the rapid development of mobile communication, the ultrawideband (UWB) positioning technology has drawn considerable attention in smartphone applications due to its merits, such as wide bandwidth, strong penetration capability, and high transmission rate [1], [2], [3], [4], [5]. Various antennas have been presented and adopted in UWB positioning systems [6], [7], [8], [9], [10]. Among them, dual-band circular-polarized (DBCP) antennas are preferred [11], [12], [13], [14], [15]. On the one hand, circular-polarized antennas hold emphatic features to avert polarization mismatch in the signal propagation process [16], [17], [18]. On the other hand, the antennas with dual-band performance have the ability to prevent interferences with designated or undesirable bands [19], [20], [21]. However, the space allocated to the antenna inside the smartphone is limited [22], [23], [24], [25]. As a feasible solution to realize a DBCP antenna in space-limited smartphone systems, the antenna can be located on the flexible printed circuit (FPC) clamped between the glass back cover and battery, as shown in Fig. 1. Due to the FPC requirements, the antenna is expected with the characteristics of ultralow profile, compact size, and integration capability with the metal ground.

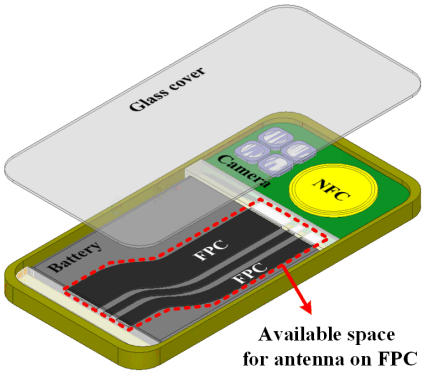

Fig. 1. Application scenarios of the proposed antenna based on FPC technology.

Recently, numerous DBCP antennas have been investigated with various methods [26], [27], [28], [29], [30], [31], [32], [33], [34], [35], [36]. The first one is to combine a wideband circular-polarized antenna with bandstop filters. With this method, a wideband microstrip antenna obtains dual-band property by etching two slots serving as bandstop structure and circular polarization by etching two gaps surrounding these two slots [26]. As another general method for more compact volume, two individual circular-polarized antenna elements operating at different bands are collocated together for DBCP radiation. A DBCP antenna is proposed by using two stacked patches with an etched slot [27]. Double-layer DBCP antenna is proposed with a lower slot-carved patch and an upper chamfered patch [28]. For the purpose of further integration, the third method is exciting two modes under different frequencies in a single antenna. A cavity-backed slot antenna with DBCP properties and a profile of $0.06\lambda_0$ is

Manuscript received 25 November 2022; revised 19 January 2023; accepted 22 January 2023. Date of publication 28 February 2023; date of current version 7 April 2023. This work was supported in part by the National Natural Science Foundation of China under Grant 62022045 and Grant U22B2016, and in part by Huawei Technologies. *(Corresponding author: Yue Li.)*

Yongjian Zhang, Yue Li, and Mingzhe Hu are with the Department of Electronic Engineering, Beijing National Research Center for Information Science and Technology, Tsinghua University, Beijing 100084, China (e-mail: lyee@tsinghua.edu.cn).

Pengfei Wu is with the Consumer Business Group, Department of Wireless Technology, Huawei Technology Company Ltd., Shanghai 201206, China (e-mail: wupengfei3@huawei.com).

Hanyang Wang is with Huawei Technologies Ltd., RG2 6AD Reading, U.K. (e-mail: hanwanga@gmail.com).

Color versions of one or more figures in this article are available at https://doi.org/10.1109/TAP.2023.3247130.

Digital Object Identifier 10.1109/TAP.2023.3247130

TABLE I
DETAILED DIMENSIONS (UNIT:mm)

h_1	h_2	h_3	h_4	h_5	h_r
0.15	0.25	0.2	0.05	0.05	0.8

proposed in [29] by employing two annular exponential slots. The DBCP antenna design in [30] presents an Archimedean spiral patch within a profile of $0.07\lambda_0$. Hassan et al. [31] propose an antenna by adopting a patch and two collocated circles to realize DBCP property within a profile of $0.04\lambda_0$. All of the DBCP antennas mentioned above are relatively large or difficult to integrate with the complete metal ground. Therefore, it is a challenge to realize a DBCP antenna in a compact size and integrate it with complete metal ground.

In this article, a DBCP microstrip antenna with broadside radiation is proposed for the UWB positioning applications in smartphone systems. The proposed antenna is composed of a cross-slot-loaded patch, a circle of capacitive via fences, and four L-shaped probes with a sequential phase feeding network fabricated on a complete metal ground. The dual-band property is realized by exciting the patch at TM_{10} mode and antiphase TM_{20} mode with broadside radiation. The capacitive via fences are located surrounding the radiation patch for miniaturization. To realize circular polarization, four L-shaped feeding probes connected with the sequential phase feeding network are arranged symmetrically under the radiation patch. Based on the UWB positioning protocol for beam angle evaluation in both elevated and horizontal planes, a three-element antenna array is fabricated by a multilayer flexible liquid crystal polymer (LCP) manufacturing process with the dimensions of $35 \times 35 \times 0.7$ mm^3 with a 0.8-mm-thickness glass cover. The experimental results show that the antenna provides an overlapped bandwidth that satisfies the requirements of efficiency and axial ratio (AR) covering the dual widebands of 6.28–6.80 and 7.86–8.20 GHz. The proposed DBCP antenna presents the merits of ultralow profile, compact size, and wide operating bandwidth.

II. ANTENNA CONFIGURATION

Fig. 2 illustrates the proposed multilayer DBCP antenna. The proposed antenna is held by six dielectric layers, named glass cover layer and Layers 1–5, respectively. The glass cover layer is constructed by WL TP-1/2 with $\varepsilon_r = 7.0$, $\tan\delta = 0.001$, and thickness $h_r = 0.8$ mm. The Layers 1–5 with different values of thickness listed in Table I are all the LCP dielectric substrates with $\varepsilon_r = 2.9$ and $\tan\delta = 0.002$.

As depicted in Fig. 2, the proposed DBCP microstrip antenna consists of a cross-slot-loaded patch, a circle of capacitive via fence, and four L-shaped probes with a sequential phase feeding network fabricated on a complete metal ground. The radiation patch etched by a cross slot is fabricated on the upper side of Layer 1. By using the L-shaped feeding probe, the patch can be excited at TM_{10} mode and antiphase TM_{20} mode, which are both with broadside radiation properties. The capacitive via fences are constructed on the upper side of Layer 2 and through Layers 2 and 3. By adjusting

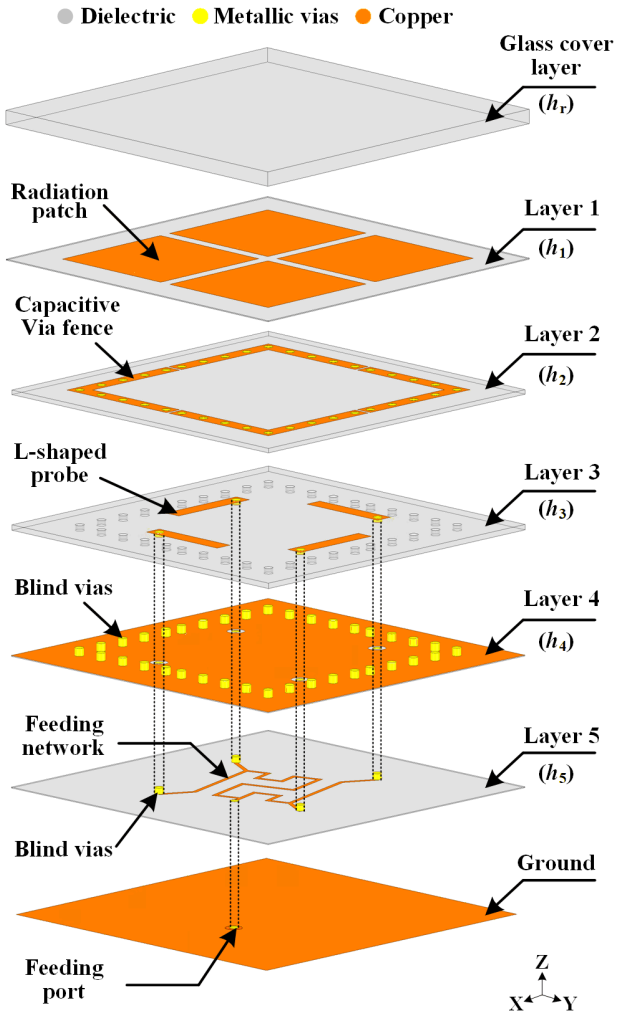

Fig. 2. Exploded view of the proposed antenna configuration.

the distance between the radiation patch and via fences, i.e., the thickness of Layer 1 h_1, the whole antenna footprint can be miniaturized for space-limited smartphone systems. The four L-shaped probes are composed of four narrow strips fabricated on the upper side of Layer 3 and four yellow blind vias connected with the sequential phase feeding network fabricated on the upper side of Layer 5. These feeding structures cooperate together to achieve circular polarization with wide AR bandwidth and wide AR beamwidth. The whole antenna with a profile of $0.8 + 0.7 = 1.5$ mm is integrated with a complete metal ground fabricated on the lower side of Layer 5. Detailed dimensions of each layer are illustrated in Fig. 3.

III. ANTENNA EVOLUTION

The design flow of the proposed DBCP antenna is shown in Fig. 4. First, a square patch (orange part) is etched by a cross slot. This patch is fed by an L-shaped probe that consists of a narrow strip (blue part) and blind via (yellow part). Then, a dual-band linear-polarized property can be realized by Antenna 1 with TM_{10} and antiphase TM_{20} modes. Second, Antenna 2 adopts a circle of via fence serving as capacitive

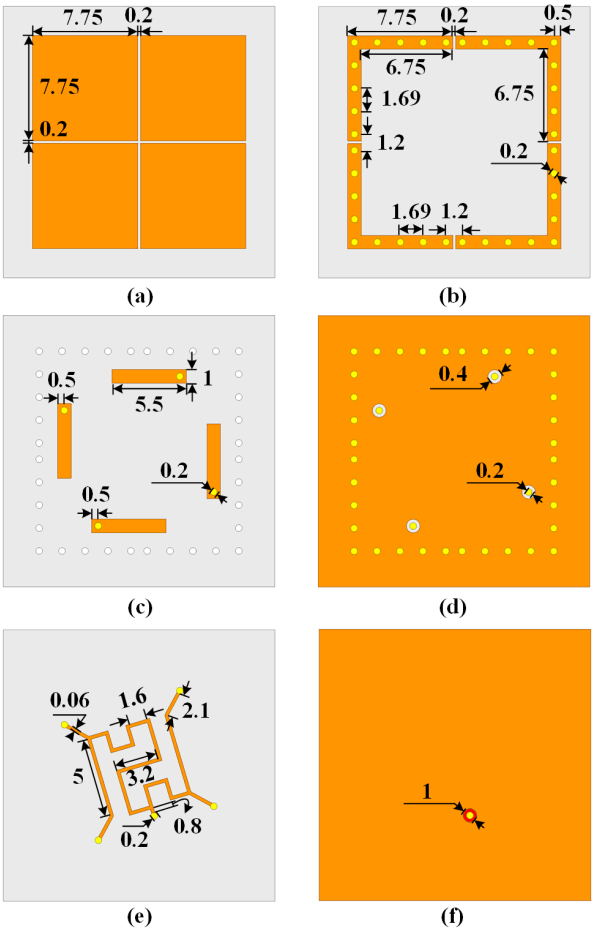

Fig. 3. Top view of the proposed antenna on (a) Layer 1, (b) Layer 2, (c) Layer 3, (d) Layer 4, (e) Layer 5, and (f) Ground.

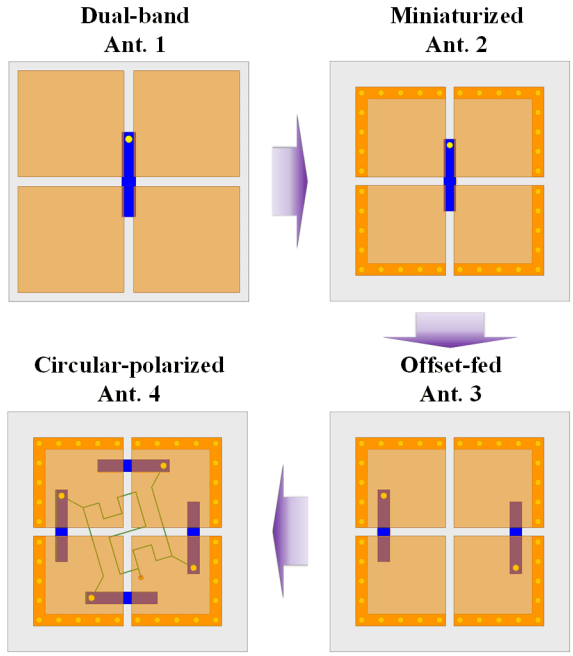

Fig. 4. Design flow of the proposed DBCP antenna.

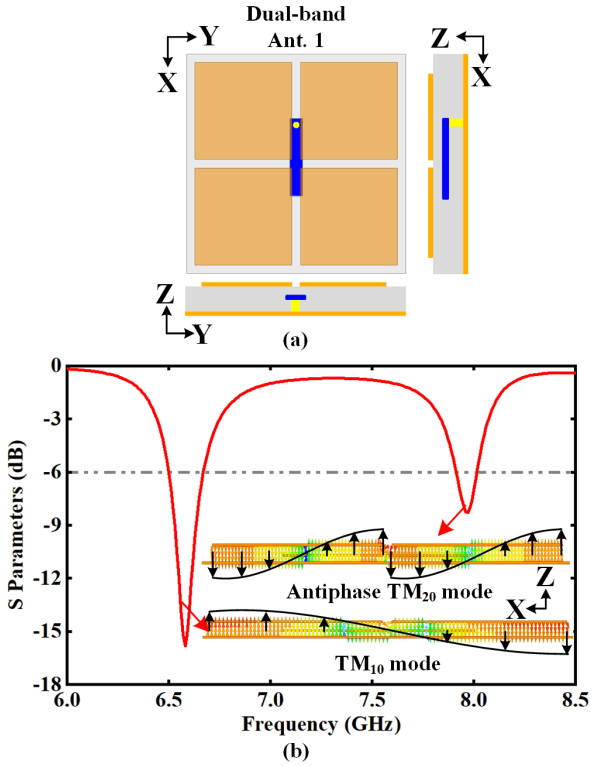

Fig. 5. Dual-band antenna design. (a) Configurations of Antenna 1 for dual bands. (b) Reflection coefficient of Antenna 1.

loading at a proper distance below the radiation patch for footprint miniaturization. Third, for circular polarization, the single L-shaped probe is replaced by dual offset-arranged L-shaped feeding probes for low cross-polarization level in the linear-polarized Antenna 3. Finally, four L-shaped probes with a sequential phase feeding network are used instead in Antenna 4. By optimizing the detailed parameters of these structures, the proposed antenna provides circular polarization in dual widebands. It should be noted that Antennas 1–4 are all analyzed under the glass cover layer, which is omitted for brevity in Fig. 4.

A. Step 1: Dual-Band Design

Fig. 5 illustrates the configuration of dual-band Antenna 1. As shown in Fig. 5(a), the cross-slot-loaded patch is fed by a single L-shaped feeding probe. By adjusting this feeding probe and optimizing the impedance matching, the linear-polarized Antenna 1 operates in dual bands near 6.5 and 8.0 GHz, with the simulated reflection coefficient result depicted in Fig. 5(b). The electric fields at these two frequencies are shown in Fig. 5(b) (inset). As seen, the electric field under the patch is half-wavelength distributed along the direction of the L-shaped probe, indicating that Antenna 1 operates at a regular TM_{10} mode at 6.5 GHz. At the high frequency, due to the loading of the L-shaped feeding probe, a reversal of the electric field will be generated at the position of the feeding probe, hence providing an electric field distribution with one-wavelength distribution but reversed in the middle line [37]. Fig. 5(b) shows that Antenna 1 operates at antiphase TM_{20} mode at

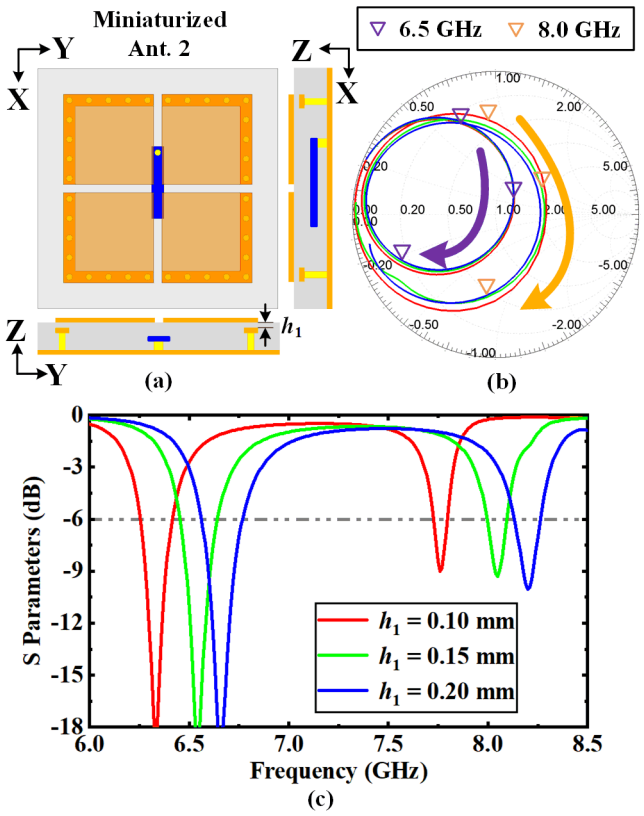

Fig. 6. Miniaturized antenna design. (a) Configurations of Antenna 2. (b) Smith chart and (c) reflection coefficient curves with different values of h_1.

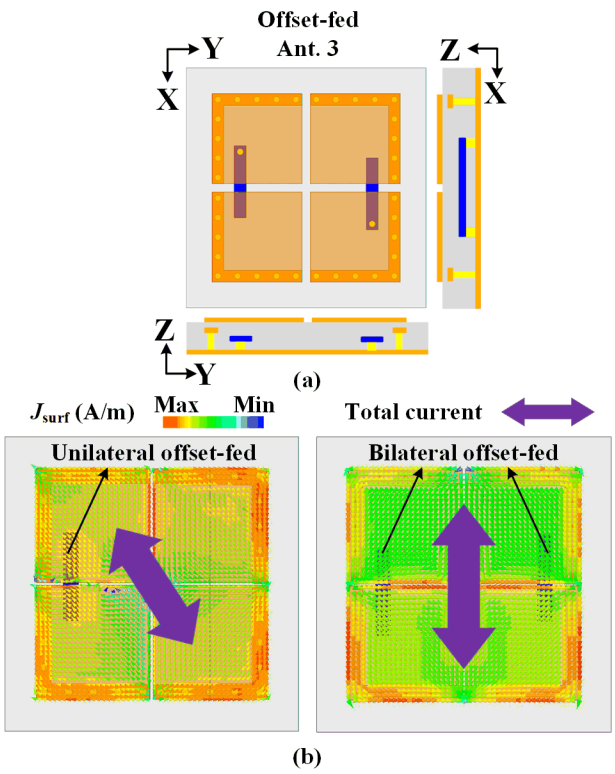

Fig. 7. Offset antenna design. (a) Configurations of Antenna 3. (b) Surface current distribution with different feeding states.

8.0 GHz. Therefore, Antenna 1 provides dual-band operation by a cross-slot-loaded patch fed by an L-shaped feeding probe.

B. Step 2: Miniaturized Design

The design strategy of miniaturized Antenna 2 is clarified in Fig. 6. On the basis of Antenna 1, Antenna 2 shown in Fig. 6(a) uses a circle of via fence arranged surrounding the cross-slot-loaded patch and at a certain distance h_1 below the patch. To more clearly explain the reason for miniaturization, the critical parameters of the via fence are investigated. As an example, the Smith chart and reflection coefficient curves with different values of distance between the radiation patch and via fence h_1 are plotted in Fig. 6(b) and (c). As seen, a larger parallel capacitance [shown as the purple and orange arrows in Fig. 6(b)] is obtained by decreasing the value of h_1 from 0.20 to 0.10 mm, and the center frequency point of TM_{10} mode or antiphase TM_{20} mode is switched to be a lower frequency. Therefore, Antenna 2 can realize different levels of miniaturization by regulating the parameters of the capacitive via fence.

C. Step 3: Offset Design

To achieve circular polarization, an offset is introduced in Antenna 3 on the basis of Antenna 2, as shown in Fig. 7. When the single L-shaped probe in Antenna 2 deviates from the central axis gradually, it is seen that inclined current distribution occurs along the patch surface, as depicted in Fig. 7(b). This physical phenomenon indicates that a cross-polarized component is introduced in the unilateral offset-fed antenna scheme, which is not suitable for the next step of circular polarization. To avoid this, a bilateral offset-fed scheme is used. As shown in Fig. 7(a), dual centrosymmetric L-shaped probes are located below the radiation patch. It can be observed that the total current is vertically distributed along the patch surface without the horizontal component, providing a pure linear polarization with broadside radiation. Besides, it is worth pointing out that the resonant frequency points of dual operating modes also deviate from the desired UWB frequency band in the unilateral offset-fed scheme. This frequency deviation can also be corrected by adjusting the positions and sizes of the dual L-shaped feeding probes, which provides a possibility for the next circular-polarized design step.

D. Step 4: Circular-Polarized Design

On the basis of offset-fed Antenna 3, the circular polarization is realized in Antenna 4 shown as Fig. 8(a). A group of rotationally symmetric L-shaped probes is adopted and arranged below the radiation patch. A four-way sequential phase feeding network (green part) with one input port (named as Port 1) and four output ports (named as Ports 2–5) is located below the probes, where these four output ports are connected with the blind vias of four probes. To meet the FPC requirement with whole metal ground, the feeding network is based on stripline structure. To begin with, the simulated

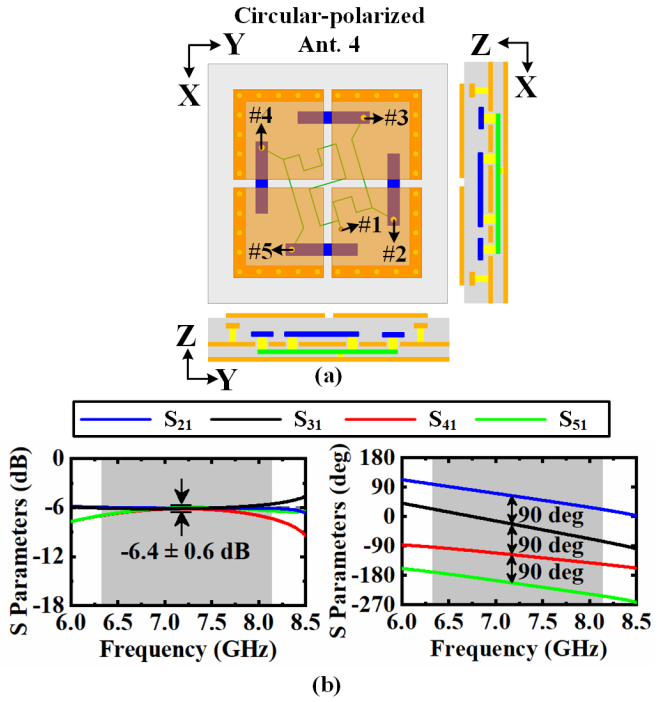

Fig. 8. Circular-polarized antenna design. (a) Configurations of Antenna 4. (b) *S* parameters of the proposed sequential phase feeding network.

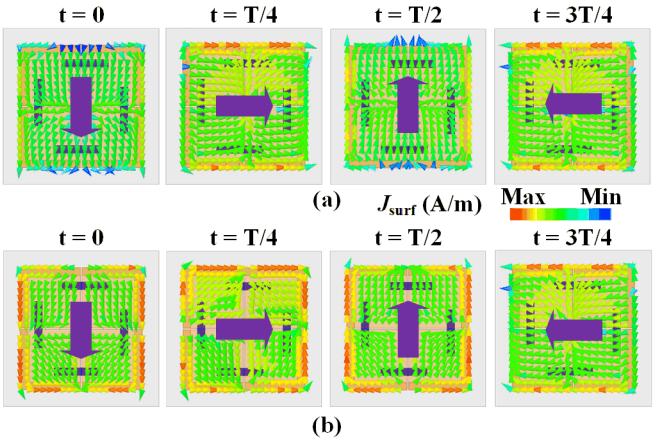

Fig. 9. Current distributions of Antenna 4 at (a) 6.5 GHz and (b) 8.0 GHz.

S parameters of an individual sequential phase feeding network are analyzed and plotted in Fig. 8(b). As seen, the power levels of the received signal on four output ports are all in the range of -6.4 ± 0.6 dB, which indicates that the radio frequency energy input from Port 1 is equally divided into four output ports. Besides, a 90° phase step is further achieved on Ports 2–5, providing a proper phase distribution for the antenna feeding structure.

Moreover, to get a straightforward view of circular-polarized radiation, the time-variant simulation of the surface current density distribution over the radiation patch is shown in Fig. 9. The current distribution is shown at the center frequency points of dual operating modes for time variation (t) of 0, T/4, T/2, and 3T/4. As t increases from 0 to 3T/4, the direction of the surface current vector rotates anticlockwise at 6.5 GHz, which indicates that the polarization sense

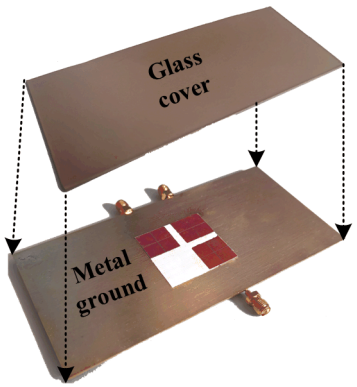

Fig. 10. Photograph of the fabricated antenna.

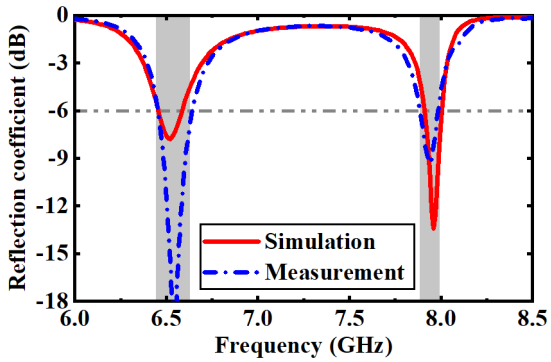

Fig. 11. Reflection coefficient of the proposed DBCP antenna.

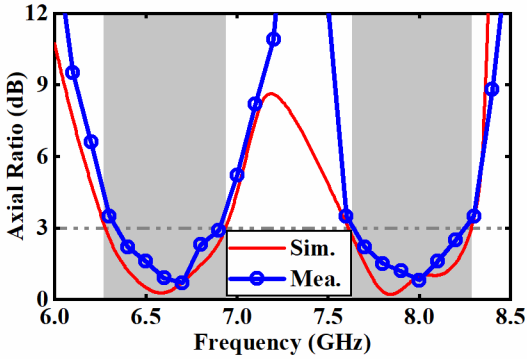

Fig. 12. AR value of the proposed DBCP antenna element.

of Antenna 4 is right-handed circular-polarized in the $+z$-direction. Similarly, the direction of the surface current vector also rotates anticlockwise at 8.0 GHz. Hence, by using four L-shaped probes and the sequential phase feeding network, a right-handed circular-polarized radiation property is realized in Antenna 4, which is adopted as the final design, i.e., the proposed antenna element in this article. The size of the metal ground scarcely affects the radiation performance, indicating that the proposed DBCP antenna is compatible with the metal ground of different sizes.

IV. Experimental Results

On the basis of the proposed antenna element above, a prototype of a three-element antenna array is built and tested

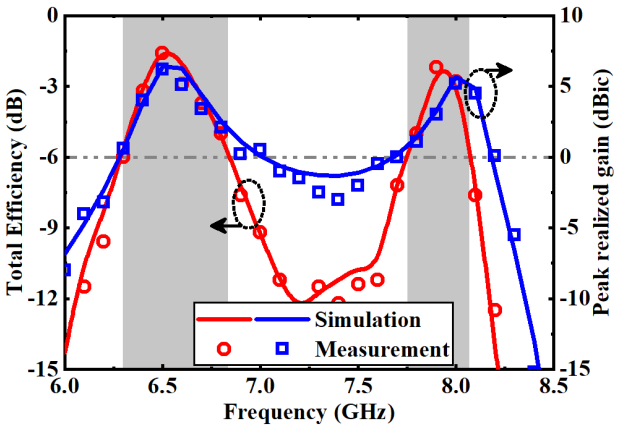

Fig. 13. Total efficiency and peak realized gain of the proposed antenna.

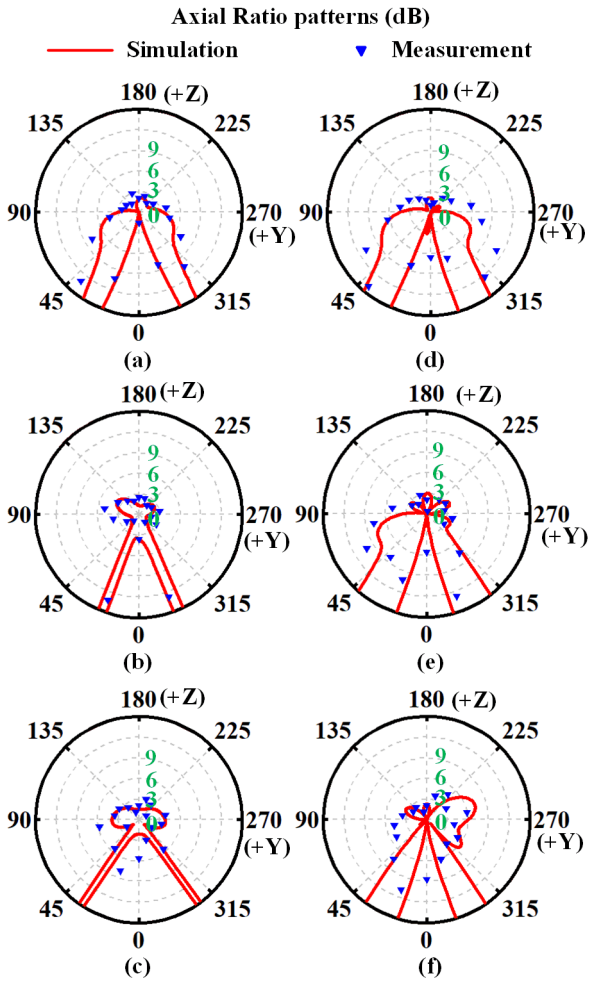

Fig. 14. AR patterns of the proposed antenna. (a) 6.3, (b) 6.5, (c) 6.7, (d) 7.9, (e) 8.0, and (f) 8.1 GHz.

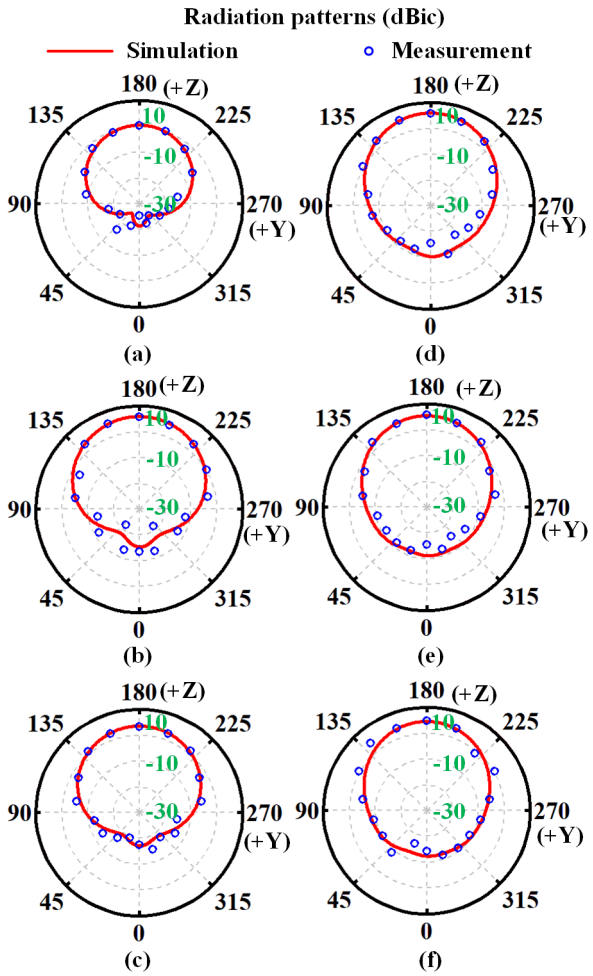

Fig. 15. Radiation patterns of the proposed antenna. (a) 6.3, (b) 6.5, (c) 6.7, (d) 7.9, (e) 8.0, and (f) 8.1 GHz.

to verify the design method for UWB positioning systems. As shown in Fig. 10, the proposed antenna array is composed of three identical DBCP antenna elements, which are located at three corners of a square dielectric substrate ($\varepsilon_r = 2.9$ and $\tan\delta = 0.002$) fabricated by the flexible LCP manufacturing process. The antenna array is clamped tightly between the WL TP-1/2 glass cover ($\varepsilon_r = 7.0$, $\tan\delta = 0.001$, and thickness $h_r = 0.8$ mm) and a large rectangular metal ground with the dimensions of 140 × 70 mm^2. Each antenna element is fed by a corresponding 50 Ω semi-grid cable.

The reflection coefficient results of a single antenna element in simulation and measurement are plotted in Fig. 11. Due to the dual operating modes, the proposed antenna realizes the measured −6 dB impedance bandwidth of 6.46–6.64 and 7.89–7.98 GHz, which is a little wider than the simulated one of 6.46–6.58 and 7.91–8.0 GHz. The difference between the simulation and measurement mainly contributes to the handmade fabrication errors and the dielectric loss. The AR values of the proposed DBCP antenna element are depicted in Fig. 12. Owing to the sequential phase feeding network, an acceptable circular-polarized behavior is obtained within the ultralow profile. As seen, the proposed antenna achieves the measured 3 dB AR bandwidth of 6.30–6.90 and 7.70–8.30 GHz. Besides, the total efficiency and peak realized gain of the proposed antenna in simulated and measured results are depicted in Fig. 13. The −6 dB efficiency bandwidths are 6.30–6.80 and 7.75–8.10 GHz. The overlapped bandwidth satisfying the requirements of efficiency and AR covers the bands of 6.30–6.80 and 7.75–8.10 GHz, which covers the

TABLE II
COMPARISONS OF THE PROPOSED ANTENNA WITH OTHER DBCP PROTOTYPES IN THE LITERATURE

Ref.	Footprint (λ_0^2)	Profile (λ_0)	3-dB AR Bandwidth (GHz)		Gain (dBic)		Integration with ground
			Lower band	Higher band	Lower band	Higher band	
[11]	0.33×0.33	0.12	1.18~1.26 (6.56%)	1.49~1.61 (7.74%)	7.72	8.11	Yes
[12]	0.90×0.90	0.32	2.27~2.54 (11.22%)	5.6~6.2 (10.49%)	3.2	8.5	No
[26]	0.85×0.43	0.02	4.0~4.6 (13.7%)	6.07~7.13 (16.6%)	6.66	5.06	No
[27]	0.25×0.25	0.055	3.48~3.52 (1.0%)	5.71~5.88 (3.1%)	N.A.	N.A.	Yes
[28]	0.23×0.23	0.02	N.A.	N.A.	N.A.	N.A.	Yes
[32]	0.75×0.75	0.065	2.238~2.285 (2.1%)	2.645~2.695 (2.0%)	3.68	3.17	No
This work	0.34×0.34	0.015	6.30~6.80 (7.6%)	7.75~8.10 (4.4%)	6.0	5.2	Yes

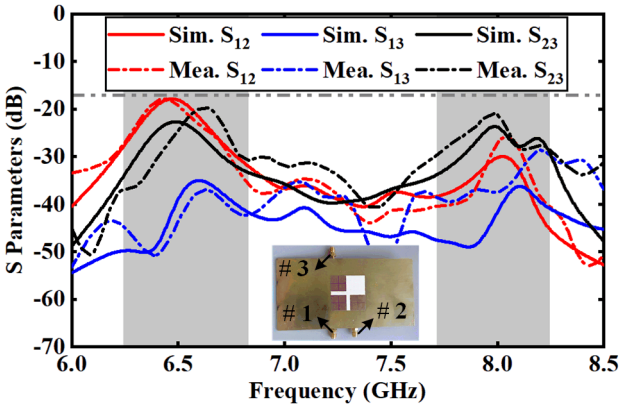

Fig. 16. Port isolations of the proposed antenna array.

desired bands in Channels 5 and 9 introduced in the UWB standards of IEEE 802.15.1-2015 and 802.15.4z. Besides, the peak realized gains are given in Fig. 13. Similarly, the proposed antenna element provides a peak gain higher than 1.2 dBic in the low band and 0.8 dBic in the high band.

The AR and radiation patterns of the proposed antenna at dual bands are illustrated in Figs. 14 and 15, respectively. In the low-frequency band of 6.30–6.80 GHz, the antenna achieves a 3 dB beamwidth of 76° and a 3 dB AR beamwidth wider than 100°. In the high-frequency band of 7.75–8.10 GHz, a 3 dB beamwidth of 78° and a 3 dB AR beamwidth wider than 60° are realized in the proposed antenna. Hence, it can be observed that the proposed DBCP antenna element provides circular polarization with broadside radiation.

The port isolation value is measured and shown in Fig. 16. In the desired operating bands, the isolation between any two ports is higher than 17 dB. The reason behind this phenomenon is that the electric field concentrates mainly on the gap between the radiation patch and the capacitive via fence, which reduces the coupling between two adjacent antenna elements.

The key performances of the proposed antenna are listed in Table II and compared with other DBCP antenna designs in the reported literatures. The antennas in [11], [12], and [26] realize wider 3 dB AR bandwidth at the cost of occupying a larger footprint or higher profile. Besides, the designs in [12] and [26] cannot be integrated with a complete metal ground. Several more compact antennas proposed in [27], [28], and [32] achieve circular-polarized radiation with only a narrow AR bandwidth. Hence, compared with the other DBCP antenna designs, the proposed microstrip antenna provides better circular-polarized radiation in dual bands with the merits of both compact volume and integration capability with the complete metal ground.

V. CONCLUSION

In this article, a DBCP microstrip antenna is proposed with an ultralow profile of $0.015\lambda_0$ and a compact footprint area of $0.76\lambda_0 \times 0.76\lambda_0$ at the frequency of 6.5 GHz. By exploiting the cross-slot-loaded patch and a circle of capacitive via fence, the antenna is miniaturized in dual desired UWB bands. Four L-shaped probes with a sequential phase feeding network are properly arranged in a rotationally symmetrical distribution, realizing circular polarization with broadside radiation. The simulated and measured results show that the proposed antenna obtains realized gain higher than 1.2 and 0.8 dBic in dual overlapped operating bands of 6.30–6.80 and 7.75–8.10 GHz, respectively. The proposed DBCP antenna is with the merits of compact footprint, ultralow profile, and integration capability with the complete metal ground, exhibiting promising potential for space-limited smartphone UWB positioning systems.

REFERENCES

[1] H. Zhang, W. Li, and T. A. Gulliver, "Pulse position amplitude modulation for time-hopping multiple-access UWB communications," *IEEE Trans. Commun.*, vol. 53, no. 8, pp. 1269–1273, Aug. 2005.

[2] S. Bastiaens et al., "Experimental benchmarking of next-gen indoor positioning technologies (unmodulated) visible light positioning and ultra-wideband," *IEEE Internet Things J.*, vol. 9, no. 18, pp. 17858–17870, Sep. 2022.

[3] W. Jiang, Z. Cao, B. Cai, B. Li, and J. Wang, "Indoor and outdoor seamless positioning method using UWB enhanced multi-sensor tightly-coupled integration," *IEEE Trans. Veh. Technol.*, vol. 70, no. 10, pp. 10633–10645, Oct. 2021.

[4] T. Liu, B. Li, and L. Yang, "Phase center offset calibration and multipoint time latency determination for UWB location," *IEEE Internet Things J.*, vol. 9, no. 18, pp. 17536–17550, Sep. 2022.

[5] X. Zhu, J. Yi, J. Cheng, and L. He, "Adapted error map based mobile robot UWB indoor positioning," *IEEE Trans. Instrum. Meas.*, vol. 69, no. 9, pp. 6336–6350, Sep. 2020.

[6] X. Shan and Z. Shen, "Miniaturized UHF/UWB tag antenna for indoor positioning systems," *IEEE Antennas Wireless Propag. Lett.*, vol. 18, no. 12, pp. 2453–2457, Dec. 2019.

[7] Y. A. Andreev, V. N. Kornienko, and S. Liu, "Method for radiation center position measurements of a combined antenna in the pulsed mode," *IEEE Trans. Antennas Propag.*, vol. 66, no. 8, pp. 4269–4276, Aug. 2018.

[8] Y. Pan and Y. Dong, "Low-profile low-cost ultra-wideband circularly polarized slot antennas," *IEEE Access*, vol. 7, pp. 160696–160704, 2019.

[9] G. P. Pochanin et al., "Measurement of coordinates for a cylindrical target using times of flight from a 1-transmitter and 4-receiver UWB antenna system," *IEEE Trans. Geosci. Remote Sens.*, vol. 58, no. 2, pp. 1363–1372, Feb. 2020.

[10] B. Hanssens et al., "An indoor variance-based localization technique utilizing the UWB estimation of geometrical propagation parameters," *IEEE Trans. Antennas Propag.*, vol. 66, no. 5, pp. 2522–2533, May 2018.

[11] S. Lee, Y. Yang, K.-Y. Lee, and K. C. Hwang, "Dual-band circularly polarized annular slot antenna with a lumped inductor for GPS application," *IEEE Trans. Antennas Propag.*, vol. 68, no. 12, pp. 8197–8202, Dec. 2020.

[12] P. Janpangngern, D. Torrungrueng, M. Krairiksh, and C. Phongcharoenpanich, "Dual-band circularly polarized omni-directional biconical antenna with double-circular parallelepiped elements for WLAN applications," *IEEE Access*, vol. 10, pp. 31970–31980, 2022.

[13] H. Nakano, T. Abe, and J. Yamauchi, "A small metaline array antenna for circularly polarized dual-band beam-steering," *IEEE Access*, vol. 10, pp. 73317–73325, 2022.

[14] M. Zada, I. A. Shah, and H. Yoo, "Metamaterial-loaded compact high-gain dual-band circularly polarized implantable antenna system for multiple biomedical applications," *IEEE Trans. Antennas Propag.*, vol. 68, no. 2, pp. 1140–1144, Feb. 2020.

[15] Y.-X. Sun, K. W. Leung, and J. Ren, "Dual-band circularly polarized antenna with wide axial ratio beamwidths for upper hemispherical coverage," *IEEE Access*, vol. 6, pp. 58132–58138, 2018.

[16] Y. Li, Z. N. Chen, X. Qing, Z. Zhang, J. Xu, and Z. Feng, "Axial ratio bandwidth enhancement of 60-GHz substrate integrated waveguide-fed circularly polarized LTCC antenna array," *IEEE Trans. Antennas Propag.*, vol. 60, no. 10, pp. 4619–4626, Oct. 2012.

[17] Y. Li, Z. Zhnag, and Z. Feng, "A sequential-phase feed using a circularly polarized shorted loop structure," *IEEE Trans. Antennas Propag.*, vol. 61, no. 3, pp. 1443–1447, Mar. 2013.

[18] C. J. Deng, Y. Li, Z. J. Zhang, and Z. H. Feng, "A wideband sequential-phase fed circularly polarized patch array," *IEEE Trans. Antennas Propag.*, vol. 62, no. 7, pp. 3890–3893, Jul. 2014.

[19] F. Liu, J. Guo, L. Zhao, G.-L. Huang, Y. Li, and Y. Yin, "Dual-band metasurface-based decoupling method for two closely packed dual-band antennas," *IEEE Trans. Antennas Propag.*, vol. 68, no. 1, pp. 552–557, Jan. 2020.

[20] W. Sun, Y. Li, L. Chang, H. Li, X. Qin, and H. Wang, "Dual-band dual-polarized microstrip antenna array using double-layer gridded patches for 5G millimeter-wave applications," *IEEE Trans. Antennas Propag.*, vol. 69, no. 10, pp. 6489–6499, Oct. 2021.

[21] Y. Qin, R. Li, Q. Xue, X. Zhang, and Y. Cui, "Aperture-shared dual-band antennas with partially reflecting surfaces for base-station applications," *IEEE Trans. Antennas Propag.*, vol. 70, no. 5, pp. 3195–3207, May 2022.

[22] Y. Li, Z. Zhang, J. Zheng, Z. Feng, and M. F. Iskander, "A compact hepta-band loop-inverted F reconfigurable antenna for mobile phone," *IEEE Trans. Antennas Propag.*, vol. 60, no. 1, pp. 389–392, Jan. 2012.

[23] C. Deng, Y. Li, Z. Zhang, and Z. Feng, "A novel low-profile hepta-band handset antenna using modes controlling method," *IEEE Trans. Antennas Propag.*, vol. 63, no. 2, pp. 799–804, Feb. 2015.

[24] L. Chang, Y. Yu, K. Wei, and H. Wang, "Polarization-orthogonal co-frequency dual antenna pair suitable for 5G MIMO smartphone with metallic bezels," *IEEE Trans. Antennas Propag.*, vol. 67, no. 8, pp. 5212–5220, Aug. 2019.

[25] H. Li, Y. Li, L. Chang, W. Sun, X. Qin, and H. Wang, "A wideband dual-polarized endfire antenna array with overlapped apertures and small clearance for 5G millimeter-wave applications," *IEEE Trans. Antennas Propag.*, vol. 69, no. 2, pp. 815–824, Feb. 2021.

[26] J. K. Deegwal and V. Sharma, "Dual band circular polarized printed dipole antenna for S and C band wireless applications," *Prog. Electromagn. Res. C*, vol. 105, pp. 129–146, 2020.

[27] P. Nayeri, K.-F. Lee, A. Z. Elsherbeni, and F. Yang, "Dual-band circularly polarized antennas using stacked patches with asymmetric U-slots," *IEEE Antennas Wireless Propag. Lett.*, vol. 10, pp. 492–495, 2011.

[28] S. Kumar, B. K. Kanaujia, M. K. Khandelwal, and A. K. Gautam, "Stacked dual-band circularly polarized microstrip antenna with small frequency ratio," *Microw. Opt. Technol. Lett.*, vol. 56, no. 8, pp. 1933–1937, Aug. 2014.

[29] Q. Wu, J. Yin, C. Yu, H. Wang, and W. Hong, "Low-profile millimeter-wave SIW cavity-backed dual-band circularly polarized antenna," *IEEE Trans. Antennas Propag.*, vol. 65, no. 12, pp. 7310–7315, Dec. 2017.

[30] H. Chen, Z. Zhang, and F. Lei, "A design of dual-band circularly polarized millimeter-wave microstrip antenna," in *Proc. IEEE Int. Symp. Antennas Propag. USNC/URSI Nat. Radio Sci. Meeting*, Jul. 2018, pp. 1827–1828.

[31] O. H. Hassan, S. I. Shams, and A. M. M. A. Allam, "Dual-band circularly polarized antenna with CPW feeding structuree," in *Proc. Asia–Pacific Microw. Conf.*, Dec. 2010, pp. 2052–2055.

[32] C. Deng, Y. Li, Z. Zhang, G. Pan, and Z. Feng, "Dual-band circularly polarized rotated patch antenna with a parasitic circular patch loading," *IEEE Antennas Wireless Propag. Lett.*, vol. 12, pp. 492–495, 2013.

[33] G. Samanta and D. Mitra, "Dual-band circular polarized flexible implantable antenna using reactive impedance substrate," *IEEE Trans. Antennas Propag.*, vol. 67, no. 6, pp. 4218–4223, Jun. 2019.

[34] Z.-P. Zhong et al., "A compact dual-band circularly polarized antenna with wide axial-ratio beamwidth for vehicle GPS satellite navigation application," *IEEE Trans. Veh. Technol.*, vol. 68, no. 9, pp. 8683–8692, Sep. 2019.

[35] Z. Li, Y. Zhu, H. Yang, G. Peng, and X. Liu, "A dual-band omnidirectional circular polarized antenna using composite right/left-handed transmission line with rectangular slits for unmanned aerial vehicle applications," *IEEE Access*, vol. 8, pp. 100586–100595, 2020.

[36] C. Sahana and M. Jayakumar, "Dual-band circularly polarized annular ring patch antenna for GPS-aided GEO-augmented navigation receivers," *IEEE Antennas Wireless Propag. Lett.*, vol. 21, no. 9, pp. 1737–1741, Sep. 2022.

[37] W. E. I. Liu, Z. N. Chen, and X. Qing, "Broadband low-profile L-probe fed metasurface antenna with TM leaky wave and TE surface wave resonances," *IEEE Trans. Antennas Propag.*, vol. 68, no. 3, pp. 1348–1355, Mar. 2020.

Yongjian Zhang received the B.S. degree in communication engineering from Tongji University, Shanghai, China, in 2018. He is currently pursuing the Ph.D. degree in electronic engineering with Tsinghua University, Beijing, China.

His current research interests include aircraft antennas, dual-polarized antennas, and multiple-input and multiple-output (MIMO) antenna arrays.

Dr. Zhang serves as a Reviewer for the IEEE TRANSACTIONS ON ANTENNAS AND PROPAGATION, IEEE ANTENNAS AND WIRELESS PROPAGATION LETTERS, and *Microwave and Optical Technology Letters*.

Yue Li (Senior Member, IEEE) received the B.S. degree in telecommunication engineering from Zhejiang University, Hangzhou, Zhejiang, China, in 2007, and the Ph.D. degree in electronic engineering from Tsinghua University, Beijing, China, in 2012.

In June 2012, he was a Post-Doctoral Fellow with the Department of Electronic Engineering, Tsinghua University. In December 2013, he was a Research Scholar with the Department of Electrical and Systems Engineering, University of Pennsylvania, Philadelphia, PA, USA. He was also a Visiting Scholar with the Institute for Infocomm Research (I2R), A∗STAR, Singapore, in 2010, and the Hawaii Center of Advanced Communication (HCAC), University of Hawaii at Manoa, Honolulu, HI, USA, in 2012. Since January 2016, he has been with Tsinghua University, where he is currently an Assistant Professor and an Associate Professor with the Department of Electronic Engineering. He has authored and coauthored over 200 journal articles and 50 international conference papers. He holds 25 granted Chinese patents. His current research interests include metamaterials, plasmonics, electromagnetics, nanocircuits, mobile and handset antennas, multiple-input and multiple-output (MIMO) and diversity antennas, and millimeter-wave antennas and arrays.

Dr. Li was a recipient of the Issac Koga Gold Medal from URSI General Assembly in 2017; the Second Prize of Science and Technology Award of China Institute of Communications in 2017; the Young Scientist Award from the conferences of Progress in Electromagnetics Research Symposium (PIERS) 2019, International Applied Computational Electromagnetics Society Symposium (ACES) 2018, Atlantic Radio Science Conference (AT-RASC) 2018, Asia-Pacific Radio Science Conference (AP-RASC) 2016, International Symposium on Electromagnetic Theory (EMTS) 2016, and URSI General Assembly and Scientific Symposium (GASS) 2014; the Best Paper Award from the conferences of PhotonIcs & Electromagnetics Research Symposium (PIERS) 2021, International Workshop on Electromagnetics (iWEM) 2021, Asia-Pacific Conference on Antennas and Propagation (APCAP) 2020 and 2017, UK-Europe-China Workshop on Millimeter Waves and Terahertz Technologies (UCMMT) 2020, International Symposium on Antennas and Propagation (ISAP) 2019, Cross Strait Quad-Regional Radio Science and Wireless Technology Conference (CSQRWC) 2018, International Symposium on Antennas, Propagation and EM Theory (ISAPE) 2021 and 2016, International Conference on Microwave and Millimeter Wave Technology (ICMMT) 2020 and 2016, National Conference on Microwave and Millimeter Waves (NCMMW) 2018 and 2017, National Conference on Antennas (NCANT) 2019 and 2017; the Outstanding Doctoral Dissertation of Beijing Municipality in 2013; and the Principal Scholarship of Tsinghua University in 2011. He is serving as an Associate Editor for the IEEE TRANSACTIONS ON ANTENNAS AND PROPAGATION, IEEE ANTENNAS AND WIRELESS PROPAGATION LETTERS, *Microwave and Optical Technology Letters*, and *Computer Applications in Engineering Education*. He is also serving on the Editorial Board of *Scientific Reports Sensors*, and *Electronics*.

Mingzhe Hu received the B.S. degree in electronic engineering from Tsinghua University, Beijing, China, in 2022, where he is currently pursuing the Ph.D. degree in electronic engineering.

His current research interests include wideband antennas, low-profile antennas, and microstrip antennas.

Dr. Hu serves as a Reviewer for the IEEE TRANSACTIONS ON ANTENNAS AND PROPAGATION and the *Microwave and Optical Technology Letters*.

Pengfei Wu received the B.S. and M.S. degrees from Southeast University, Nanjing, China, in 2005 and 2008, respectively.

From 2009 to 2011, he was an RF Engineer to design antennas with Nokia Mobile, Amphenol, Finland. From 2012 to 2015, he joined ZTE, Shenzhen, China, as a Senior RF Engineer. He is currently an Antenna Specialist with the Consumer Business Group, Huawei Technology Company Ltd., Shanghai, China. His current research interests include broadband antennas, multiple-input multiple-output antennas, and low-profile antennas.

Hanyang Wang (Fellow, IEEE) received the Ph.D. degree from Heriot-Watt University, Edinburgh, U.K., in 1995.

From 1986 to 1991, he was a Lecturer and an Associate Professor with Shandong University, Jinan, China. From 1995 to 1999, he was a Post-Doctoral Research Fellow with the University of Birmingham, Birmingham, U.K.; and the University of Essex, Colchester, U.K. From 1999 to 2000, he was with Vector Fields Ltd., Oxford, U.K., as a Software Development and Microwave and an Antenna Engineering Consultant Engineer. He joined at Nokia U.K. Ltd., Farnborough, U.K., in 2001, where he had been a Mobile Antenna Specialist for 11 years. He joined Huawei Technologies, Reading, U.K., where he is currently the Chief Scientist of mobile terminal antennas and the Head of the Mobile Antenna Technology Division. He leads a large group of antenna experts and engineers and takes the full leadership and responsibility in the research and development of antenna technologies to guarantee the market success of all Huawei's mobile terminal products ranging from smartphones, laptops, tablets, MiFi, data cards, smart watches, BT headsets, routers, the Internet of Things (IoT), smart screens, Customer Premise Equipment (CPE), Virtual Reality (VR), and automobiles. He is also an Adjunct Professor with Nanjing University, Nanjing, China; and Sichuan University, Chengdu, China. He has authored over refereed 120 articles on these topics. He holds over 50 granted U.S./European/Japanese/Chinese patents, including 31 U.S. patents, and has more than 60 patent applications in pending. His current research interests include small, wideband, and multiband antennas for mobile terminals, multiple-input and multiple-output (MIMO) antennas and antenna arrays for 5G sub-6 GHz, and 5G millimeter-wave mobile communications.

Dr. Wang is a Huawei Fellow and an IET Fellow. He was a recipient of the Title of Nokia Inventor of the Year in 2005, the Nokia Excellence Award in 2011, the Huawei Individual Gold Medal Award in 2012, and the Huawei Team Gold Medal Award in 2013 and 2014. His patent was ranked number one among the 2015 Huawei Top Ten Patent Awards. He was an Associate Editor of the IEEE ANTENNAS AND WIRELESS PROPAGATION LETTERS from 2015 to 2021.